Letter Editors' Suggestion

Concurrence of anomalous Hall effect and charge density wave in a superconducting topological kagome metal

F. H. Yu,[1] T. Wu,[1] Z. Y. Wang,[1] B. Lei,[1] W. Z. Zhuo,[1] J. J. Ying,[1,*] and X. H. Chen[1,2,3,†]

[1]*Hefei National Laboratory for Physical Sciences at Microscale and Department of Physics, and CAS Key Laboratory of Strongly-Coupled Quantum Matter Physics, University of Science and Technology of China, Hefei, Anhui 230026, China*

[2]*CAS Center for Excellence in Quantum Information and Quantum Physics, Hefei, Anhui 230026, China*

[3]*Collaborative Innovation Center of Advanced Microstructures, Nanjing 210093, People's Republic of China*

(Received 22 February 2021; accepted 22 June 2021; published 8 July 2021)

As one of the most fundamental physical phenomena, the anomalous Hall effect (AHE) typically occurs in ferromagnetic materials but is not expected in the conventional superconductors. Here, we have observed a giant AHE in kagome superconductor CsV_3Sb_5 with transition temperature (T_c) of 2.7 K. The anomalous Hall conductivity reaches up to $2.1 \times 10^4\ \Omega^{-1}\ cm^{-1}$ which is larger than those observed in most of the ferromagnetic metals. Strikingly, the emergence of AHE exactly follows the higher-temperature charge-density-wave (CDW) transition with $T_{CDW} \sim 94$ K, indicating a strong correlation between the CDW state and AHE. Furthermore, AHE disappears when the CDW transition is completely suppressed at high pressure. The origin for AHE is attributed to enhanced skew scattering in the CDW state and large Berry curvature arising from the kagome lattice. These discoveries make CsV_3Sb_5 as an ideal platform to study the interplay among nontrivial band topology, CDW, and unconventional superconductivity.

DOI: 10.1103/PhysRevB.104.L041103

A kagome lattice, representing a two-dimensional network with corner-sharing triangles, provides a fertile ground to study the frustrated, novel correlated and topological electronic states owing to its unusual lattice geometry [1–3]. In general, kagome lattice naturally possesses Dirac dispersion and flat bands that promote an electronic correlation effect [4]. Thus, in principle, kagome lattice can exhibit a large variety of electronic instabilities. Many exotic quantum phenomena have been observed in magnetic kagome metals, including the giant anomalous Hall effect (AHE) [5–12], chiral edge state [13,14], and topological surface Fermi arcs [15,16]. Up to now, exploring exotic properties in kagome lattice remains quite challenging, particularly for multiple electronic orders.

Recently, a family of quasi-two-dimensional kagome metals AV_3Sb_5 (A = K, Rb, Cs) have attracted tremendous attention [17]. These materials crystallize in the $P6/mmm$ space group with ideal kagome nets of V atoms which are coordinated by Sb atoms. The kagome layers are sandwiched by extra antimonene layers (Sb2) and Cs layers as shown in Fig. 1(a).The resistivity of the AV_3Sb_5 family exhibits anomalies at T^* ranging from 78 to 110 K, which are ascribed to the formation of charge density wave (CDW) order [17,18]. The observation of superconductivity in the stoichiometric AV_3Sb_5 with kagome lattice [19–21] makes this family an ideal playground to study the correlation among superconductivity, CDW, and nontrivial band topology. For example, topological charge order was recently reported in KV_3Sb_5 [18] and signatures of spin-triplet superconductivity were also claimed in Nb-$K_{1-x}V_3Sb_5$ devices [22]. Recent reports have shown an unconventional giant AHE in nonsuperconducting $K_{1-x}V_3Sb_5$ which is attributed to the skew scattering of spin cluster [23]. However, no signature of long-ranged magnetic order or localized magnetic moments has been observed in a near-stoichiometric sample by muon spin resonance (μSR) measurements [24]. One explanation for the aforementioned discrepancy of AHE is attributed to the vacancies at A sites [20]. These vacancies might lead to additional local moments around vacancies that gives rise to the giant AHE but are detrimental for the superconductivity. In fact, superconductivity in this family seems to be very fragile by involving the vacancies of alkali metal [20]. Therefore, whether such a large AHE is universal for the AV_3Sb_5 family and its correlation with the emergent orders needs to be elucidated. Here, we observed the giant AHE in the superconducting CsV_3Sb_5 with the highest T_c of 2.7 K in the AV_3Sb_5 family. The anomalous Hall conductivity reaches up to $2.1 \times 10^4\ \Omega^{-1}\ cm^{-1}$, which is larger than those observed in most of the ferromagnetic metals [25]. More interestingly, it is clearly evidenced that the AHE develops spontaneously with the occurrence of CDW, indicating a strong correlation between the AHE and CDW state. Such concurrence of CDW and SC behavior is also confirmed in the high-pressure experiments.

Single crystals of CsV_3Sb_5 were synthesized via a self-flux growth method similar to the previous reports [19]. In order to prevent the reaction of Cs with air and water, all the preparation processes were performed in an argon glovebox. After high-temperature reaction in the furnace, the excess flux is removed by using water and a millimeter-sized

*yingjj@ustc.edu.cn
†chenxh@ustc.edu.cn

 ©2021 American Physical Society

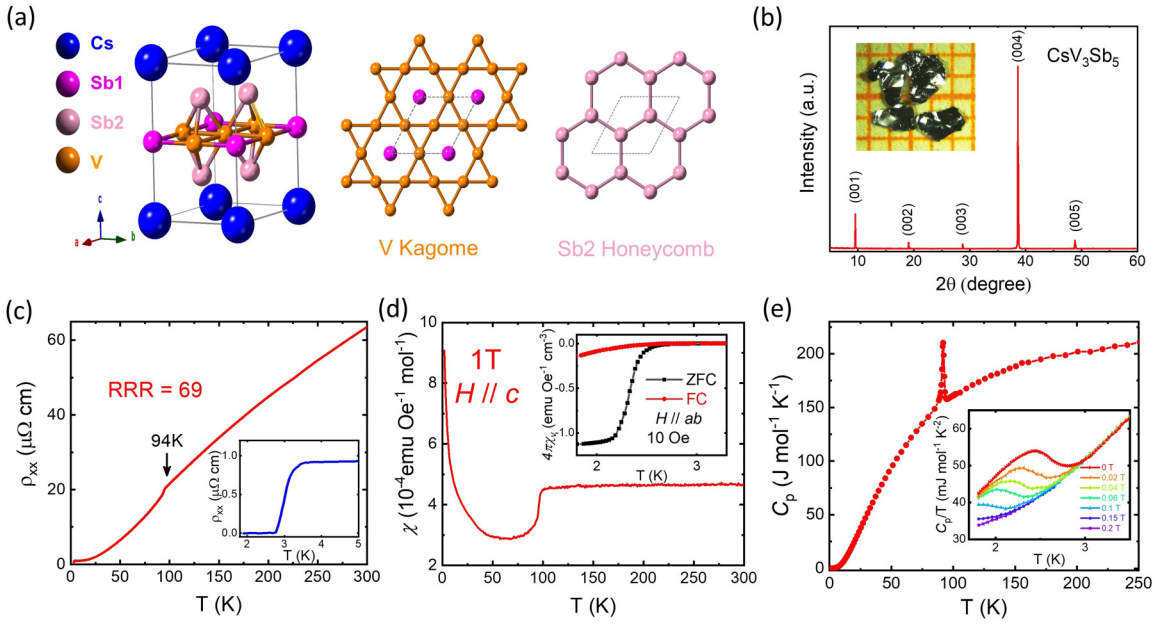

FIG. 1. (a) Crystal structure of CsV_3Sb_5. The vanadium sublattice forms perfect kagome lattice. There are two distinct Sb sublattices. Sb1 atom is centered on each kagome hexagon and Sb2 sublattice creates an antimonene layer below and above each kagome layer. (b) X-ray diffraction pattern of CsV_3Sb_5 single crystal with the corresponding Miller indices (00L) in parentheses. The inset shows photo of typical CsV_3Sb_5 single crystals on a 1 mm grid paper. (c)–(e) Temperature dependence of resistivity, magnetization, and heat capacity of CsV_3Sb_5 single crystal. Clear phase transition around 94 K was observed in all measurements, possibly related to the charge density wave. The insets represent the bulk superconductivity around 2.7 K in all the measurements.

single crystal can be obtained. The as-grown CsV_3Sb_5 single crystals are stable in the air. X-ray diffraction data are collected at room temperature by using an x-ray diffractometer (SmartLab-9, Rikagu) with Cu K_α radiation. Electrical transport and heat capacity measurements were carried out in a Quantum Design physical property measurement system (PPMS-14T). The longitudinal resistance and Hall resistance were simultaneously measured with standard six-probe Hall bar geometry. Magnetization measurements were performed in SQUID magnetometer (MPMS-5 T, Quantum Design). A piston cylinder cell (PCC) was used to generate hydrostatic pressure above 2 GPa for the high-pressure electrical transport measurements. Daphne 7373 was used as the pressure transmitting medium in the PCC. The pressure values in the PCC were determined from the superconducting transition of Sn [26].

The crystal structure of CsV_3Sb_5 is presented in Fig. 1(a). Figure 1(b) displays the x-ray diffraction pattern of a CsV_3Sb_5 single crystal. Only (00l) diffraction peaks can be detected, indicating the pure phase of the as-grown single crystal with a [001] preferred orientation. The c-axis lattice parameter is determined to be 9.308 Å, which is consistent with the previously reported value of CsV_3Sb_5 [17]. As shown in Figs. 1(c)–1(e), the resistivity, magnetic susceptibility, and heat capacity all show a phase transition around 94 K which is ascribed to a CDW-like transition. Meanwhile, bulk superconductivity with T_c of 2.7 K is also observed, being consistent with previous measurements [19]. The residual resistivity ratio is 69, indicating the high quality of the measured single crystal. The large anisotropy of the upper critical field (see Fig. S1 in the Supplemental Material [27]) indicates a two-dimensional (2D) nature, which is consistent with the predicted 2D electronic structure in CsV_3Sb_5 [19].

To further elucidate its electronic properties, we have performed magnetoresistance measurement under external magnetic field along both the c axis and the ab plane, and the results are shown in Figs. 2(a) and 2(b), respectively. Large MR ($= [\rho(H) - \rho(0)]/\rho(0)$) and clear Shubnikov–de Haas (SdH) quantum oscillations (QOs) can be clearly observed at low temperatures with external magnetic field along the c axis. In principle, the Fourier transform of QOs can provide useful insight into the Fermi surfaces. As shown in the inset of Fig. 2(c), the MR curves above 2 T can be well fitted by using a polynomial formula. After subtracting a slowly changed background, the oscillating parts of resistivity $\Delta\rho_{xx}$ as a function of $1/(\mu_0 H)$ at several representative temperatures are extracted and shown in Fig. 2(c). The fast Fourier transform (FFT) of the QOs reveals four principal frequencies at 18, 26, 72, and 92 T. In contrast, only two frequencies were detected in previous reports on $K_{1-x}V_3Sb_5$ and RbV_3Sb_5 samples [21,23]. Since $F1$ and $F2$, $F3$, and $F4$ are rather close to each other, the doubling of the frequency numbers can be attributed to the slightly warping of FSs along the c-axis direction. All these frequencies are smaller than that observed in the $K_{1-x}V_3Sb_5$ and RbV_3Sb_5 samples, indicating that CsV_3Sb_5 has the smallest extremal orbits of Fermi surfaces in this family. The effective mass can be extracted from the temperature dependence of the amplitude of FFT peak using the Lifshitz-Kosevich (LK) formula [28]. The oscillation amplitude at a fixed magnetic field is proportional to the thermal damping factor R_T: $R_T = \frac{\alpha m^* T}{B\sinh(\alpha m^* T/B)}$, where $\alpha = 14.69\,\mathrm{T/K}$ is a constant, $B = \mu_0 H$ is the magnetic flux

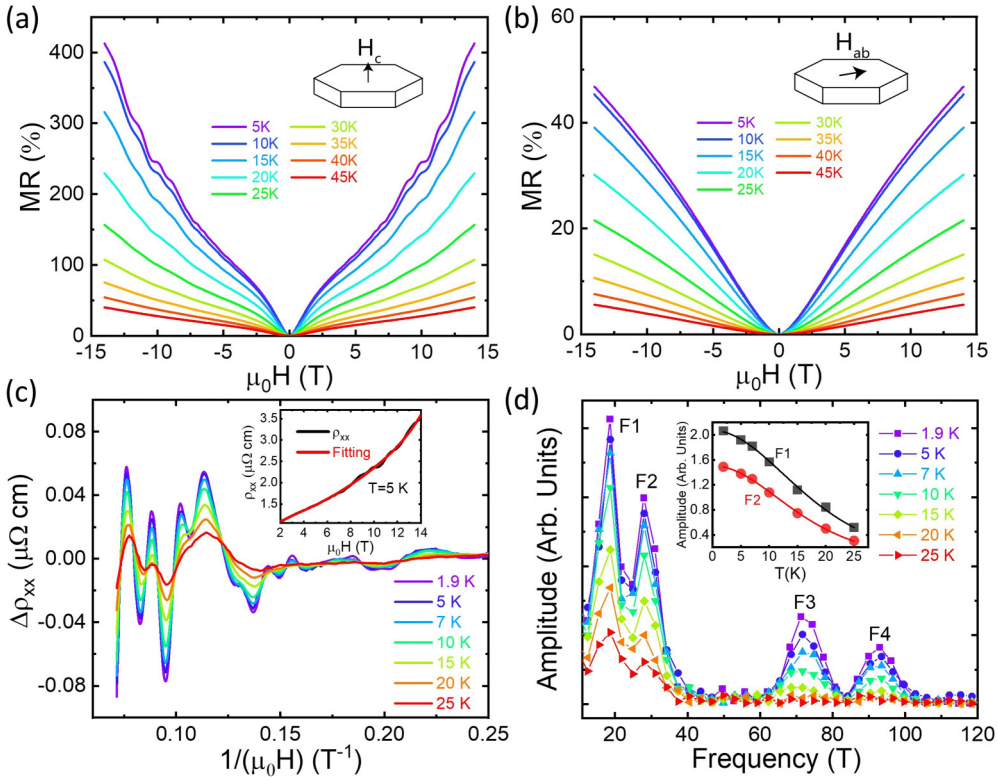

FIG. 2. Magnetoresistance measured at various temperatures with magnetic field along c axis (a) and in ab plane (b), respectively. (c) Magnetoresistance after subtracting a monotonic background plotted as a function of $1/(\mu_0 H)$ at various temperatures. The inset shows a polynomial fitting of a MR curve above 2 T. (d) Extracted fast Fourier transform frequency showing four principal frequencies. The inset shows the Lifshitz-Kosevich fit of the $F1$ and $F2$ orbits to extract the effective mass.

density (taking the average value of the field window used for the FFT of QOs), and $m^* = m/m_e$ is the cyclotron mass ratio (m_e is the mass of free electron). The temperature dependence of FFT amplitude of $F1$ and $F2$ can be fitted very well as shown in the inset of Fig. 2(d), and yields effective mass to be $0.028m_e$ and $0.031m_e$ for $F1$ and $F2$ orbitals, respectively. The small extremal cross sections of FSs accompanying light effective mass could be related to the highly dispersive bands in CsV_3Sb_5.

In order to check the AHE in CsV_3Sb_5, we have performed the Hall effect measurements at various temperatures as shown in Figs. 3(a) and 3(b). ρ_{xy} exhibits a linear behavior at high temperature, indicating that the carrier density is dominated by one band. ρ_{xy} gradually deviates the linear behavior and the slope of high-field ρ_{xy} gradually decreases below T^* and changes its sign around 35 K. The magnitude of the Hall coefficient reaches its maximum value around T^*, as shown in the inset of Fig. 3(b), similar to the cases of $K_{1-x}V_3Sb_5$ [23] and RbV_3Sb_5 [21]. Since CsV_3Sb_5 is a multiband system, such behaviors could be attributed to the significant enhancement of hole mobility at low temperature [21]. In the low-field region, highlighted by the gray shading area in Fig. 3(a), an antisymmetric sideways "S" line shape is observed, which is similar to that reported in the $K_{1-x}V_3Sb_5$ sample. We extract ρ_{xy}^{AHE} by subtracting the local linear ordinary Hall term (typically from 1 to 2 T at low temperature) as shown in Figs. 3(c) and 3(d). ρ_{xy}^{AHE} decreases with increasing the temperature and persists up to the CDW transition temperature T^*. We also obtain the Hall conductivity by inverting the resistivity matrix, $\sigma_{xy} = -\rho_{xy}/({\rho_{xx}}^2 + {\rho_{xy}}^2)$. The anomalous Hall conductivity (AHC) σ_{AHE} is obtained by subtracting the linear local ordinary Hall conductivity background (for details see Fig. S4 in the Supplemental Material [27]). As shown in Fig. S2 of the Supplemental Material [27], the angle-dependent σ_{AHE} can't be linearly scaled with an out-of-plane component of magnetic field, which excludes normal Hall effect as a possible origin.

One remarkable observation here is that the AHE emerges simultaneously with the CDW transition. To confirm such correlation between CDW and AHE is intrinsic rather than coincident in this type of material. We use high pressure to directly tune the T^* and check whether AHE is concurrent with CDW order. In Fig. 4(a), T^* can be suppressed to 33 K with the pressure around 1.42 GPa, similar to the previous high-pressure results [29,30]. With temperature below T^*, the Hall resistivity exhibits an antisymmetric sideways "S" line shape in the low-field region as shown in Fig. 4(b), which is the same as the case at ambient pressure. The anomalous Hall conductivity has been extracted as shown in Fig. 4(c), which clearly shows the sudden appearance of the AHE below T^*. Further increasing the pressure to 2.02 GPa, the CDW can be completely suppressed as shown in Fig. S5 of the Supplemental Material [27]. In the meantime, the AHE disappears and the Hall resistivity can be well fitted by using the two-band model as shown in Fig. S7. Our high-pressure transport measurements confirm that the CDW and AHE occur at the same time similar to the case of the ambient pressure.

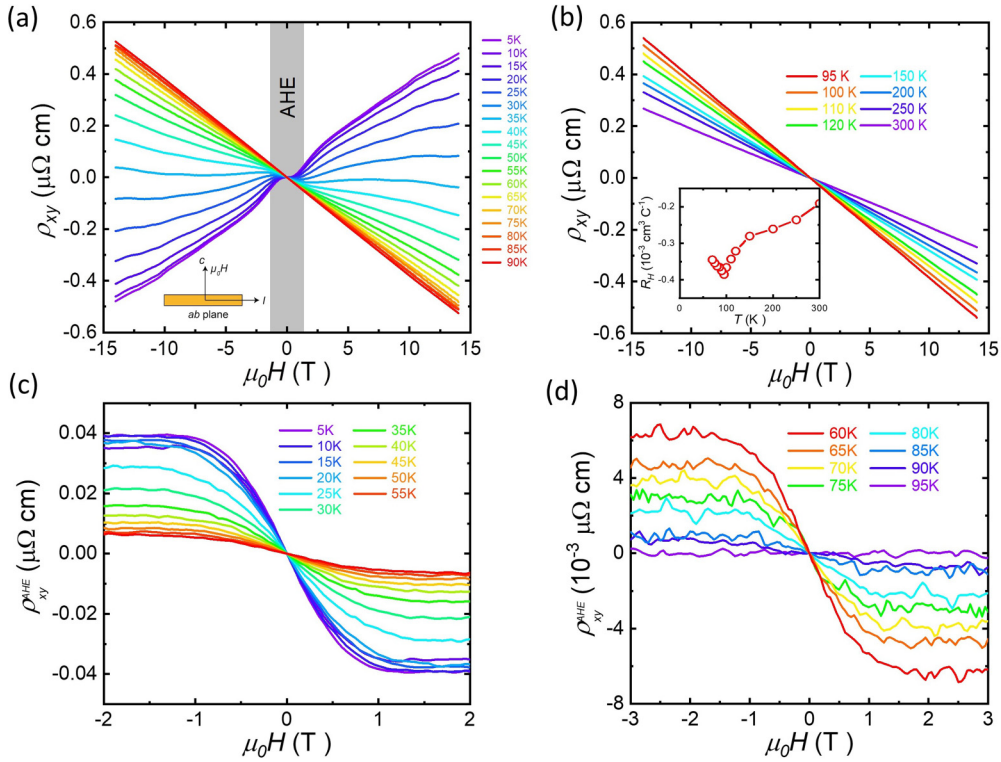

FIG. 3. (a),(b) Field dependence of Hall resistivity at various temperatures with magnetic field up to 14 T. The gray area represents the AHE in the low-field region. The inset shows the temperature dependence of Hall coefficient. The magnitude of R_{H} reaches its maximum value around T^*. (c),(d) Extracted ρ_{xy}^{AHE} by subtracting the local linear ordinary Hall background at various temperatures. AHE spontaneously emerges below T^*.

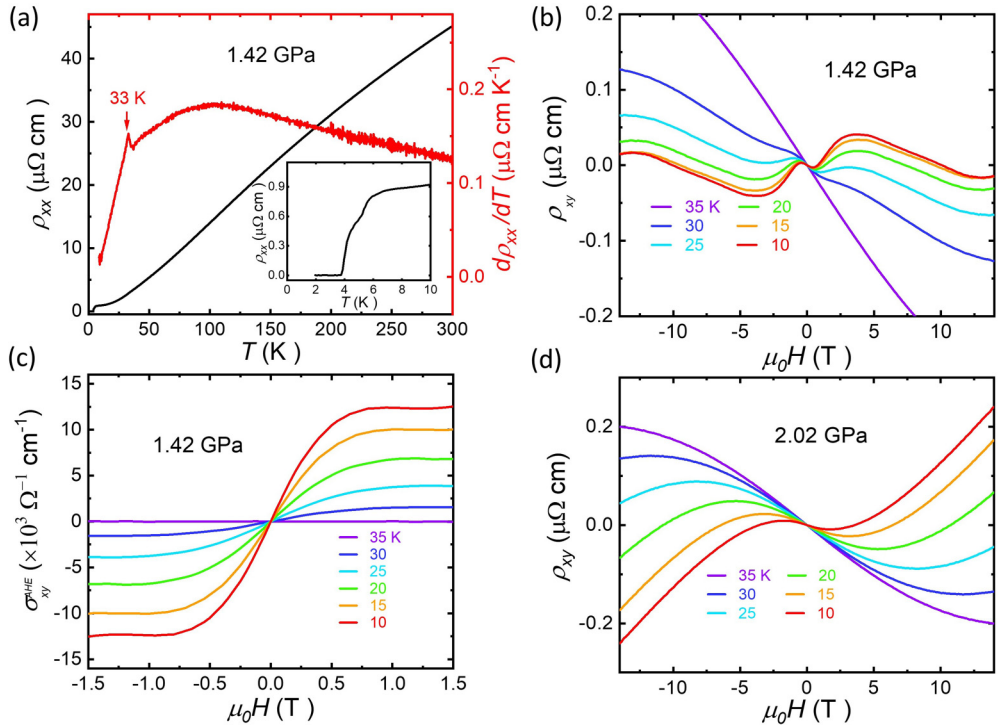

FIG. 4. (a) Temperature dependence of the resistivity curve for CsV_3Sb_5 at 1.42 GPa. T^* is suppressed to 33 K as determined from the derivative resistivity curve. The inset exhibits the superconducting transition at 1.42 GPa. (b) Hall resistivity at various temperatures under the pressure of 1.42 GPa. The AHE sudden appears below T^*. (c) The extracted anomalous Hall conductivity at various temperatures. (d) The Hall resistivity at various temperatures with the pressure of 2.02 GPa. No AHE is observed since CDW is completely suppressed.

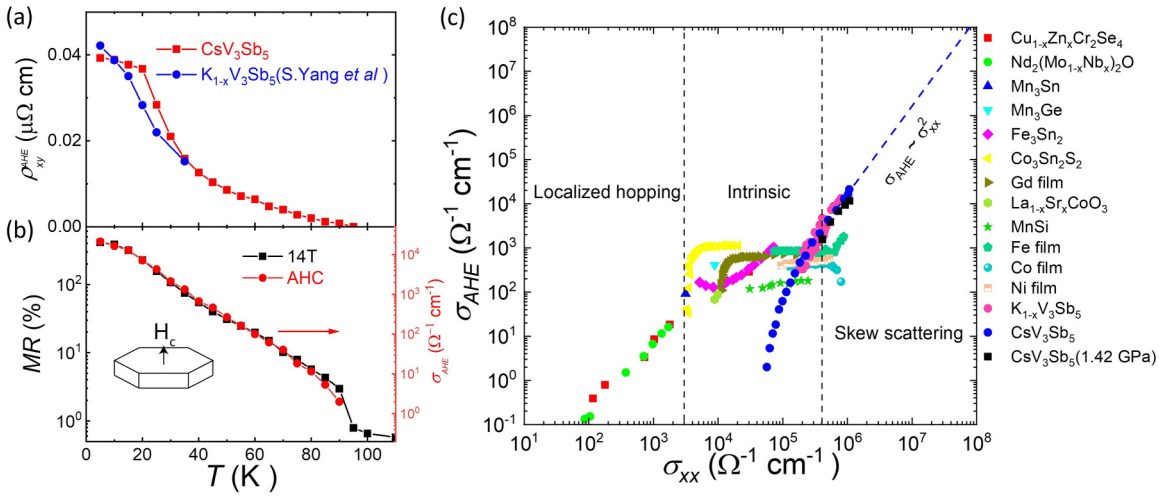

FIG. 5. (a) The ρ_{xy}^{AHE} as a function of temperature for CsV_3Sb_5 and $K_{1-x}V_3Sb_5$. The data of $K_{1-x}V_3Sb_5$ is taken from Ref. [23]. (b) Scaling behavior of magnetoresistance at 14 T with σ_{AHE} for CsV_3Sb_5. (c) σ_{AHE} versus σ_{xx} for a variety of materials comparing with CsV_3Sb_5 spanning various regimes from localized hopping regime to the skew scattering regime. For CsV_3Sb_5, σ_{AHE} follows quadratic scaling with σ_{xx} only at low temperature and locates at the same position with $K_{1-x}V_3Sb_5$.

With temperature decreasing below T^*, ρ_{xy}^{AHE} at ambient pressure exhibits a rapid increase around 20–40 K as shown in Fig. 5(a). Such a behavior is qualitatively similar to that previously reported in $K_{1-x}V_3Sb_5$. The MR at 14 T is plotted as a function of temperature as shown in Fig. 5(b). The MR shows a sudden jump below T^* indicating its strong correlation with the CDW order. The carrier mobility is enhanced and the scattering can be effectively suppressed when entering the CDW state, thus giving rise to the enhancement of MR. More interestingly, below T^*, σ_{AHE} can be well scaled with MR as shown in Fig. 5(b). All these discoveries indicate that the origin of AHE should correlate strongly with CDW order in the AV_3Sb_5 system. To further understand the AHE in CsV_3Sb_5, we have plotted σ_{AHE} versus σ_{xx} together with a variety of other typical AHE materials as shown in Fig. 5(c) [5,6,8,10,23,31,32]. Various AHE regimes from the localized hopping regime to the skew scattering regime are divided by considering the value of σ_{xx}. follows quadratic scaling with σ_{xx} below 45 K and locates at almost the same position with $K_{1-x}V_3Sb_5$. However, at higher temperature, σ_{AHE} severely deviates from the σ_{xx}^2 behavior. Meanwhile, the σ_{AHE} for CsV_3Sb_5 at 1.42 GPa also locates at the same position as that at ambient pressure. These results indicate that AHE is universal in the AV_3Sb_5 family. It may be from complex origins by involving both Berry curvature and skew scattering. Next, we will discuss this issue in more detail.

In a short summary, a giant σ_{AHE} is revealed in a kagome superconductor CsV_3Sb_5, an AHE material which shows bulk superconductivity. Usually AHE occurs with broken time-reversal symmetry, typically in a ferromagnetic phase which is not favored for conventional superconductivity. The discovery of AHE in the superconducting kagome metal indicates that either superconductivity or AHE hosts an unconventional mechanism in this type of material. AHE is usually ascribed to the Berry curvature of band structure in magnetic phase or electron scattering due to magnetic impurities [25,33]. According to the underlying mechanism, the AHE can be roughly divided into intrinsic and extrinsic categories. The intrinsic AHE is related to the band structure and proportional to the integral of Berry curvatures below Fermi level. Large intrinsic AHE has been widely observed in the magnetic topological materials such as $Co_3Sn_2S_2$ [8,9] and Co_2MnGa [11,12]. In our case, when CDW transition occurs, a gap may open on the topological band which could introduce a large Berry curvature in this system, leading to the giant AHE. In fact, scanning tunneling microscopy measurements find evidence that the CDW state displays a chiral anisotropy with an energy gap opening at Fermi level [18]. However, the calculated intrinsic AHE based on realistic parameters is much smaller than the AHE observed in our experiment [18], indicating that the intrinsic AHE mechanism alone can't give a satisfactory explanation. The extrinsic AHE depends on asymmetric electrons scattering in the periodic potential of a crystal, which is usually caused by magnetic impurities [25]. The skew scattering from disorder tends to dominate the AHE in highly conductive ferromagnets. The giant AHE at low temperature in CsV_3Sb_5 locates in the skew scattering region and follows the σ_{xx}^2 behavior as shown in Fig. 5(c), indicating that the main contribution of AHE at low temperature comes from the skew scattering [23,34,35]. Since orbital magnetoresistance also depends on the electron scattering, it can qualitatively well explain the scaling behavior between MR and AHE. Since the superconducting CsV_3Sb_5 is likely nonmagnetic and the local moment is absent in KV_3Sb_5 indicated by the μSR experiments [24], the mechanism of skew scattering in this system is still not well understood. However, tiny amounts of paramagnetic impurities may exist in the single crystal judging from the Curie-Weiss tail in the magnetic susceptibility curve below 50 K [Fig. 1(d)], almost the same temperature below which σ_{AHE} rapidly increases and follows quadratic scaling with σ_{xx}. By fitting the susceptibility at low temperatures with the Curie-Weiss law, we can estimate the level of paramagnetic impurity to be 0.7%.

It would be interesting for the theorists to figure out whether a large extrinsic AHE could originate from such a low level of paramagnetic impurities in a kagome metal. The unusual lattice geometry of the kagome lattice intertwined with the CDW state could be the possible origin of large skew scattering. Quantitative understanding for the giant AHE observed in the AV_3Sb_5 family and its correlation with superconductivity, CDW, and topological states still needs further investigation.

In conclusion, we observed a giant AHE in superconducting CsV_3Sb_5 single crystals with kagome lattice. The concurrence of AHE and CDW indicates the unconventional origin of AHE, which may be possibly related to the enhanced skew scattering in the CDW state and large Berry curvature due to kagome lattice. Our work suggests unconventional superconductivity in CsV_3Sb_5 and stimulates broad interest in studying the correlation between the CDW state and AHE in the kagome materials.

This work was supported by the National Key Research and Development Program of the Ministry of Science and Technology of China (Grants No. 2019YFA0704901 and No. 2017YFA0303001), the Anhui Initiative in Quantum Information Technologies (Grant No. AHY160000), the Science Challenge Project of China (Grant No. TZ2016004), the Key Research Program of Frontier Sciences, CAS, China (Grant No. QYZDYSSWSLH021), the Strategic Priority Research Program of the Chinese Academy of Sciences (Grant No. XDB25000000), the National Natural Science Foundation of China (Grants No. 11888101 and No. 11534010), and the Fundamental Research Funds for the Central Universities (Grants No. WK3510000011 and No. WK2030020031).

[1] Y. Zhou, K. Kanoda, and T.-K. Ng, Rev. Mod. Phys. **89**, 025003 (2017).
[2] T.-H. Han, J. S. Helton, S. Chu, D. G. Nocera, J. A. Rodriguez-Rivera, C. Broholm, and Y. S. Lee, Nature (London) **492**, 406 (2012).
[3] S. Sachdev, Phys. Rev. B **45**, 12377 (1992).
[4] I. I. Mazin, H. O. Jeschke, F. Lechermann, H. Lee, M. Fink, R. Thomale, and R. Valentí, Nat. Commun. **5**, 4261 (2014).
[5] S. Nakatsuji, N. Kiyohara, and T. Higo, Nature (London) **527**, 212 (2015).
[6] A. K. Nayak, J. E. Fischer, Y. Sun, B. Yan, J. Karel, A. C. Komarek, C. Shekhar, N. Kumar, W. Schnelle, J. Kübler, C. Felser, and S. S. P. Parkin, Sci. Adv. **2**, e1501870 (2016).
[7] K. Kuroda, T. Tomita, M. T. Suzuki, C. Bareille, A. A. Nugroho, P. Goswami, M. Ochi, M. Ikhlas, M. Nakayama, S. Akebi, R. Noguchi, R. Ishii, N. Inami, K. Ono, H. Kumigashira, A. Varykhalov, T. Muro, T. Koretsune, R. Arita, S. Shin *et al.*, Nat. Mater. **16**, 1090 (2017).
[8] E. Liu, Y. Sun, N. Kumar, L. Muechler, A. Sun, L. Jiao, S.-Y. Yang, D. Liu, A. Liang, Q. Xu, J. Kroder, V. Süß, H. Borrmann, C. Shekhar, Z. Wang, C. Xi, W. Wang, W. Schnelle, S. Wirth, Y. Chen, S. T. B. Goennenwein, and C. Felser, Nat. Phys. **14**, 1125 (2018).
[9] Q. Wang, Y. Xu, R. Lou, Z. Liu, M. Li, Y. Huang, D. Shen, H. Weng, S. Wang, and H. Lei, Nat. Commun. **9**, 3681 (2018).
[10] L. Ye, M. Kang, J. Liu, F. von Cube, C. R. Wicker, T. Suzuki, C. Jozwiak, A. Bostwick, E. Rotenberg, D. C. Bell, L. Fu, R. Comin, and J. G. Checkelsky, Nature (London) **555**, 638 (2018).
[11] K. Manna, Y. Sun, L. Muechler, J. Kübler, and C. Felser, Nat. Rev. Mater. **3**, 244 (2018).
[12] A. Sakai, Y. P. Mizuta, A. A. Nugroho, R. Sihombing, T. Koretsune, M.-T. Suzuki, N. Takemori, R. Ishii, D. Nishio-Hamane, R. Arita, P. Goswami, and S. Nakatsuji, Nat. Phys. **14**, 1119 (2018).
[13] J.-X. Yin, W. Ma, T. A. Cochran, X. Xu, S. S. Zhang, H.-J. Tien, N. Shumiya, G. Cheng, K. Jiang, B. Lian, Z. Song, G. Chang, I. Belopolski, D. Multer, M. Litskevich, Z.-J. Cheng, X. P. Yang, B. Swidler, H. Zhou, H. Lin, T. Neupert, Z. Wang, N. Yao, T.-R. Chang, S. Jia, and M. Zahid Hasan, Nature (London) **583**, 533 (2020).
[14] J.-X. Yin, S. S. Zhang, H. Li, K. Jiang, G. Chang, B. Zhang, B. Lian, C. Xiang, I. Belopolski, H. Zheng, T. A. Cochran, S.-Y. Xu, G. Bian, K. Liu, T.-R. Chang, H. Lin, Z.-Y. Lu, Z. Wang, S. Jia, W. Wang, and M. Z. Hasan, Nature (London) **562**, 91 (2018).
[15] N. Morali, R. Batabyal, P. K. Nag, E. Liu, Q. Xu, Y. Sun, B. Yan, C. Felser, N. Avraham, and H. Beidenkopf, Science **365**, 1286 (2019).
[16] D. F. Liu, A. J. Liang, E. K. Liu, Q. N. Xu, Y. W. Li, C. Chen, D. Pei, W. J. Shi, S. K. Mo, P. Dudin, T. Kim, C. Cacho, G. Li, Y. Sun, L. X. Yang, Z. K. Liu, S. S. P. Parkin, C. Felser, and Y. L. Chen, Science **365**, 1282 (2019).
[17] B. R. Ortiz, L. C. Gomes, J. R. Morey, M. Winiarski, M. Bordelon, J. S. Mangum, I. W. H. Oswald, J. A. Rodriguez-Rivera, J. R. Neilson, S. D. Wilson, E. Ertekin, T. M. McQueen, and E. S. Toberer, Phys. Rev. Mater. **3**, 094407 (2019).
[18] Y.-X. Jiang, J.-X. Yin, M. M. Denner, N. Shumiya, B. R. Ortiz, G. Xu, Z. Guguchia, J. He, M. Shafayat Hossain, X. Liu, J. Ruff, L. Kautzsch, S. S. Zhang, G. Chang, I. Belopolski, Q. Zhang, T. A. Cochran, D. Multer, M. Litskevich, Z.-J. Cheng *et al.*, Nat. Mater. (2021), doi:10.1038/s41563-021-01034-y.
[19] B. R. Ortiz, S. M. L. Teicher, Y. Hu, J. L. Zuo, P. M. Sarte, E. C. Schueller, A. M. M. Abeykoon, M. J. Krogstad, S. Rosenkranz, R. Osborn, R. Seshadri, L. Balents, J. He, and S. D. Wilson, Phys. Rev. Lett. **125**, 247002 (2020).
[20] B. R. Ortiz, P. M. Sarte, E. M. Kenney, M. J. Graf, S. M. L. Teicher, R. Seshadri, and S. D. Wilson, Phys. Rev. Mater. **5**, 034801 (2021).
[21] Q. Yin, Z. Tu, C. Gong, Y. Fu, S. Yan, and H. Lei, Chin. Phys. Lett. **38**, 037403 (2021).
[22] Y. Wang, S. Yang, P. K. Sivakumar, B. R. Ortiz, S. M. L. Teicher, H. Wu, A. K. Srivastava, C. Garg, D. Liu, S. S. P. Parkin, E. S. Toberer, T. McQueen, S. D. Wilson, and M. N. Ali, arXiv:2012.05898.
[23] S.-Y. Yang, Y. Wang, B. R. Ortiz, D. Liu, J. Gayles, E. Derunova, R. Gonzalez-Hernandez, L. Šmejkal, Y. Chen, S. S.

P. Parkin, S. D. Wilson, E. S. Toberer, T. McQueen, and M. N. Ali, Sci. Adv. **6**, eabb6003 (2020).

[24] E. M. Kenney, B. R. Ortiz, C. Wang, S. D. Wilson, and M. J. Graf, J. Phys.: Condens. Matter **33**, 235801 (2021).

[25] N. Nagaosa, J. Sinova, S. Onoda, A. H. MacDonald, and N. P. Ong, Rev. Mod. Phys. **82**, 1539 (2010).

[26] L. D. Jennings and C. A. Swenson, Phys. Rev. **112**, 31 (1958).

[27] See Supplemental Material at http://link.aps.org/supplemental/10.1103/PhysRevB.104.L041103 for further details on the experimental measurements.

[28] D. Shoenberg, *Magnetic Oscillations in Metals*, Cambridge Monographs on Physics (Cambridge University Press, Cambridge, UK, 1984).

[29] F. H. Yu, D. H. Ma, W. Z. Zhuo, S. Q. Liu, X. K. Wen, B. Lei, J. J. Ying, and X. H. Chen, Nat. Commun. **12**, 3645 (2021).

[30] K. Y. Chen, N. N. Wang, Q. W. Yin, Y. H. Gu, K. Jiang, Z. J. Tu, C. S. Gong, Y. Uwatoko, J. P. Sun, H. C. Lei, J. P. Hu, and J. G. Cheng, Phys. Rev. Lett. **126**, 247001 (2021).

[31] T. Miyasato, N. Abe, T. Fujii, A. Asamitsu, S. Onoda, Y. Onose, N. Nagaosa, and Y. Tokura, Phys. Rev. Lett. **99**, 086602 (2007).

[32] S. Iguchi, N. Hanasaki, and Y. Tokura, Phys. Rev. Lett. **99**, 077202 (2007).

[33] E. M. Pugh and N. Rostoker, Rev. Mod. Phys. **25**, 151 (1953).

[34] Y. Tian, L. Ye, and X. Jin, Phys. Rev. Lett. **103**, 087206 (2009).

[35] D. Hou, G. Su, Y. Tian, X. Jin, S. A. Yang, and Q. Niu, Phys. Rev. Lett. **114**, 217203 (2015).